Enhanced Kerr nonlinearity based on wave-number mismatch in hot atoms

Xueyi Jiang (江雪仪)[1] Lida Zhang (张理达)[1,*] Yueping Niu (钮月萍),[1,2,†] and Shangqing Gong (龚尚庆)[1,2,3,‡]
[1]*School of Physics, East China University of Science and Technology, Shanghai 200237, China*
[2]*Shanghai Frontiers Science Center of Optogenetic Techniques for Cell Metabolism, Shanghai 200237, China*
[3]*Hefei National Laboratory, Hefei, Anhui 230088, China*

(Received 30 September 2025; revised 2 March 2026; accepted 10 April 2026; published 7 May 2026)

Optical Kerr nonlinearity is important for various applications in both classical and quantum regimes. It has been shown that Kerr nonlinearity can be considerably enhanced based on electromagnetically induced transparency in cold atoms. However, in a hot atomic ensemble the Kerr nonlinearity is usually weakened by the Doppler effect. Here we show that the Kerr nonlinearity can be enhanced by tuning the wave-number mismatch between the probe and control fields in hot atoms. When the wave number of the control field, denoted by k_c, is larger than that of the probe field, denoted by k_p, the transition strength for the probe field from the ground to two dressed states created by the control field becomes stronger, leading to an increased nonlinear dispersion and absorption. Upon increasing the ratio k_c/k_p further, the effective number of atoms contributing to the interaction decreases such that the nonlinear dispersion and absorption are eventually reduced. Nevertheless, the peak nonlinear dispersion and absorption are enhanced by factors of up to 3 and 2, respectively, for $k_c/k_p > 1$ in comparison to the case of $k_c/k_p = 1$. Our results may be beneficial for a variety of applications where the Kerr nonlinearity is crucial.

DOI: 10.1103/77hm-ktyj

I. INTRODUCTION

The optical Kerr effect represents an important class of nonlinear phenomena that is crucial to a variety of important applications [1]. In classical optics, Kerr nonlinearity can be utilized for the realization of self-phase modulation [2–5], optical solitons [6–10], bistability [11–14], etc., while in the quantum regime, Kerr nonlinearity has been widely explored to generate quantum squeezing and entanglement [15–20] and to realize quantum nondemolition measurement [21–23].

Conventional approaches to obtain the Kerr effect are based on light-matter interaction in the far-off-resonance regime such that the material can be simply characterized by a third-order nonlinear coefficient [1]. In the far-off-resonance regime, the nonlinear coefficient is usually very weak. One of the most major developments to enhance the nonlinearity is based on electromagnetically induced transparency (EIT) [24–31]. In a typical EIT scheme consisting of a weak probe and a strong control field coupled near resonantly to atoms with a three-level structure, the control field creates two dressed eigenstates with eigenfrequencies determined by its Rabi frequency. For a resonant probe field, the transition amplitudes between the ground and the two dressed states are equal but of opposite signs, leading to destructive quantum interference such that the otherwise opaque atomic medium becomes transparent for the probe field. This subsequently allows simultaneous suppression of linear absorption and giant enhancement of Kerr nonlinearity [32–43]. In particular, it has been investigated that Kerr nonlinearity based on an EIT scheme in cold atoms can be enhanced by several orders of magnitude [32,34], highlighting its potential for nonlinearity-dependent applications.

However, in a hot atomic ensemble, one has to take into account the effect of atomic motion, which introduces the Doppler effect. Due to the Doppler effect, the eigenfrequencies of the two dressed states depend not only on the Rabi frequency of the control field but also on the velocity of the moving atoms. As velocity increases, one eigenfrequency vanishes while the other moves towards infinity, suggesting a broadened and attenuated absorption spectrum with a significantly narrowed and shallowed transparency window [44–49] and therefore a weakened Kerr nonlinearity.

Recently, it has been found that in ladder-type EIT schemes a frequency gap between the two dressed eigenstates can be created in which the probe transition is not allowed, when the wave number of control field, denoted by k_c, is larger than that of the probe, denoted by k_p [50–55]. As a result, the absorption of the probe field is considerably suppressed, thereby improving the EIT spectrum with a much deepened transparency window. Furthermore, the absorption peaks in the EIT spectrum are enhanced for $k_c/k_p > 1$ as compared to the case of $k_c/k_p \leqslant 1$, suggesting stronger interaction between the probe field and the thermal atomic ensemble in the regime of $k_c/k_p > 1$.

In particular, for a three-level ladder EIT configuration, the effect of wave-number mismatch on the EIT spectrum has been analyzed in detail [55]. It was shown that the width of the EIT window initially increases to a maximum and then gradually decreases with increasing k_c/k_p. However, the

*Contact author: zhang_lida@foxmail.com
†Contact author: niuyp@ecust.edu.cn
‡Contact author: sqgong@ecust.edu.cn

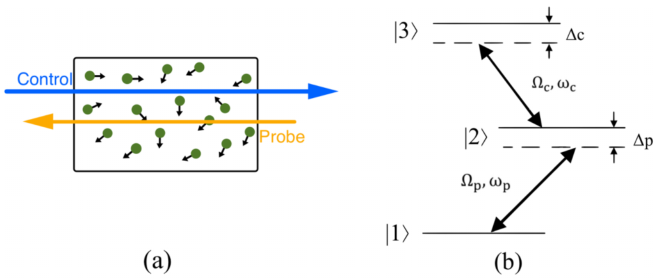

FIG. 1. (a) Counterpropagating geometry for the control and probe fields which are incident to a hot atomic ensemble where each atom has a three-level ladder-type structure as shown in (b). The probe field with Rabi frequency Ω_p and carrier frequency ω_p couples the lower transition $|1\rangle \leftrightarrow |2\rangle$, while the upper transition $|2\rangle \leftrightarrow |3\rangle$ is driven by the stronger control field denoted by its Rabi frequency Ω_c and carrier frequency ω_c.

underlying mechanism behind this behavior has not been fully elucidated. Furthermore, studies on the wave-number mismatch effect have been confined to the linear regime. It remains unclear whether a similar effect can be observed in the nonlinear regime, as nonlinear responses exhibit a more complex dependence on the Doppler effect.

In this work we explore the possibility to enhance the Kerr nonlinearity via tuning the wave-number mismatch between the two fields in a three-level ladder EIT system. We first calculate the atomic response perturbatively with respect to the weak probe field, and the resulting third-order susceptibility is analyzed under the laser geometry where the probe and control fields propagate in opposite directions. We find that in the regime of $k_c/k_p > 1$ the third-order susceptibility can be enhanced. More specifically, the Kerr dispersion can be maximally improved approximately by a factor of 3 while the Kerr absorption can be improved by around 2 times. Both the Kerr absorption and dispersion feature an initially rising and then gradually falling behavior for increasing k_c/k_p; the underlying mechanism is thoroughly explained in the dressed-state picture in terms of transition strength and effective atomic number involved in the light-atom interaction. Such a mechanism can also be employed to explain the similar behavior for the width of the EIT window as a function of k_c/k_p, as illustrated in Ref. [55].

II. THEORETICAL MODEL

We consider a three-level ladder scheme as illustrated in Fig. 1 , which has been explored previously to demonstrate improved EIT based on wave-number mismatch in a hot atomic system [50–52,55]. The two transitions $|1\rangle \leftrightarrow |2\rangle$ and $|2\rangle \leftrightarrow |3\rangle$ are coupled by the probe and control fields whose Rabi frequencies are denoted by Ω_p and Ω_c, respectively. For simplicity, Ω_p and Ω_c are assumed real in the following. The probe (control) field is detuned from the resonant transition frequency ω_{21} (ω_{32}) by $\Delta_p = \omega_p - \omega_{21}$ ($\Delta_c = \omega_c - \omega_{32}$). Here ω_p (ω_c) denotes the frequency of the probe (control) field. In the interaction picture and under the dipole and rotating-wave approximation, the Hamiltonian is given by

$$\hat{H} = \hbar \begin{bmatrix} 0 & -\Omega_p & 0 \\ -\Omega_p & -\Delta_p & -\Omega_c \\ 0 & -\Omega_c & -(\Delta_c + \Delta_p) \end{bmatrix}. \tag{1}$$

The atomic dynamics is governed by the density-matrix equation

$$\frac{d\rho}{dt} = -\frac{i}{\hbar}[\hat{H}, \rho] + L\rho, \tag{2}$$

where the first and second terms on the right-hand side describe the coherent and dissipative processes, respectively. Here the dissipative processes are mainly due to the spontaneous decay of the two excited states $|2\rangle$ and $|3\rangle$. We assume a dilute atomic gas such that the dissipation due to atomic collisions is negligible. We can then write $L\rho = L_{21}\rho + L_{32}\rho$, where

$$L_{21}\rho = \frac{\Gamma_2}{2}(2\hat{\sigma}_{21}\rho\hat{\sigma}_{12} - \hat{\sigma}_{11}\rho - \rho\hat{\sigma}_{11}), \tag{3}$$

$$L_{32}\rho = \frac{\Gamma_3}{2}(2\hat{\sigma}_{32}\rho\hat{\sigma}_{23} - \hat{\sigma}_{22}\rho - \rho\hat{\sigma}_{22}) \tag{4}$$

are the two decaying channels, respectively [56], Γ_j is the decay rate for the state $|j\rangle$ for $j \in \{2, 3\}$, and $\hat{\sigma}_{ij} = |i\rangle\langle j|$ is the atomic operator.

To calculate the atomic response for the probe field, we first obtain the related density-matrix equations

$$\dot{\rho}_{11} = i\Omega_p(\rho_{21} - \rho_{12}) + \Gamma_2\rho_{22}, \tag{5a}$$

$$\dot{\rho}_{22} = i[\Omega_p(\rho_{12} - \rho_{21}) + \Omega_c(\rho_{32} - \rho_{23})] - \Gamma_2\rho_{22} + \Gamma_3\rho_{33}, \tag{5b}$$

$$\dot{\rho}_{33} = i\Omega_c(\rho_{23} - \rho_{32}) - \Gamma_3\rho_{33}, \tag{5c}$$

$$\dot{\rho}_{21} = i[\Omega_p(\rho_{11} - \rho_{22}) + \Omega_c\rho_{31} + \Delta_p\rho_{21}] - \frac{\Gamma_2}{2}\rho_{21}, \tag{5d}$$

$$\dot{\rho}_{31} = i(\Omega_c\rho_{21} - \Omega_p\rho_{32}) + \left(i\Delta_c + i\Delta_p - \frac{\Gamma_2 + \Gamma_3}{2}\right)\rho_{31}, \tag{5e}$$

$$\dot{\rho}_{32} = i[\Omega_c(\rho_{22} - \rho_{33}) - \Omega_p\rho_{31}] + \left(i\Delta_c - \frac{\Gamma_3}{2}\right)\rho_{32}. \tag{5f}$$

We then calculate the nonlinear atomic susceptibilities for the probe field, which is determined by the atomic coherence ρ_{21}. Assuming a weak probe field such that $\Omega_p \ll \Omega_c$, the density-matrix element can be expanded in series as $\rho_{ij} = \sum_n \rho_{ij}^{(n)}$, where $\rho_{ij}^{(n)}$ is of $O(\Omega_p^n)$. Furthermore, in the limit of $\Omega_p \ll \Omega_c$, most of the atoms reside in the ground state $|1\rangle$, i.e., $\rho_{11}^{(0)} \simeq 1$, $\rho_{22}^{(0)} \simeq 0$, $\rho_{33}^{(0)} \simeq 0$, and $\sum_{j=1}^{3} \rho_{jj}^{(n)} = 0$ for $n \geqslant 1$. Then the third-order $\rho_{21}^{(3)}$, which is associated with the Kerr nonlinearity for the probe field, can be obtained as

$$\rho_{21}^{(3)} = \frac{\Omega_p\left[\left(\Delta_p + \Delta_c + i\frac{\Gamma_3}{2}\right)\left(\rho_{11}^{(2)} - \rho_{22}^{(2)}\right) + \Omega_c\rho_{32}^{(2)}\right]}{\Omega_c^2 - \left(\Delta_p + i\frac{\Gamma_2}{2}\right)\left(\Delta_p + \Delta_c + i\frac{\Gamma_3}{2}\right)}. \tag{6}$$

Here the lower-order solutions are given by

$$\rho_{22}^{(2)} = \frac{i\Omega_p\left(\rho_{12}^{(1)} - \rho_{21}^{(1)}\right)}{\Gamma_2}, \tag{7}$$

$$\rho_{33}^{(2)} = \frac{2\Omega_p\Omega_c}{D}\{(\Gamma_2+\Gamma_3)\big[2i\Omega_c\big(\rho_{12}^{(1)}-\rho_{21}^{(1)}\big) - \Gamma_2\big(\rho_{13}^{(1)}+\rho_{31}^{(1)}\big)\big] + 2i\Gamma_2\Delta_c\big(\rho_{13}^{(1)}-\rho_{31}^{(1)}\big)\}, \quad (8)$$

$$\rho_{32}^{(2)} = \frac{2\Omega_p}{D}\{\Gamma_3(\Gamma_2+\Gamma_3+2i\Delta_c)\big[\Omega_c\big(\rho_{21}^{(1)}-\rho_{12}^{(1)}\big) - i\Gamma_2\rho_{31}^{(1)}\big] + 2i\Gamma_2\Omega_c^2\big(\rho_{13}^{(1)}-\rho_{31}^{(1)}\big)\}, \quad (9)$$

$$\rho_{21}^{(1)} = \frac{2(2\Delta_p+2\Delta_c+i\Gamma_3)\Omega_p}{D_1}, \quad (10)$$

$$\rho_{31}^{(1)} = -\frac{4\Omega_c\Omega_p}{D_1}, \quad (11)$$

where $D = \Gamma_2[4\Omega_c^2(\Gamma_2+\Gamma_3)+\Gamma_3(\Gamma_2+\Gamma_3)^2+4\Gamma_3\Delta_c^2]$ and $D_1 = \Gamma_2\Gamma_3 - 2i\Gamma_2\Delta_c - 2i\Delta_p(\Gamma_2+\Gamma_3) - 4\Delta_p^2 - 4\Delta_p\Delta_c + 4\Omega_c^2$. The Kerr nonlinear susceptibility is then given by [35,36]

$$\chi_{\rm Kerr} = \frac{N|d_{12}|^4}{\varepsilon_0\hbar^3\Omega_p^3}\rho_{21}^{(3)}, \quad (12)$$

where N is the atomic density, ε_0 is the vacuum dielectric constant, and d_{12} is the electric dipole moment between state $|1\rangle$ and state $|2\rangle$. From Eqs. (6)–(11) it can be checked that $\rho_{21}^{(3)}$, which corresponds to the nonlinear polarization of the medium, is proportional to Ω_p^3. We then divide it by Ω_p^3 to obtain the Kerr susceptibility, which does not depend on the probe field itself. In the following, we assume that the lower transition for the probe field is fixed such that the dipole moment d_{12} remains unchanged. Furthermore, the atomic density and the medium length are maintained to give the same optical depth. In this way, $\chi_{\rm Kerr}$ is solely determined by $\rho_{21}^{(3)}$. We then define a rescaled Kerr nonlinearity $\chi^{(3)}$ for convenience as

$$\chi^{(3)} = \frac{\rho_{21}^{(3)}}{\Omega_p^3}. \quad (13)$$

The $\chi^{(3)}$ differs from $\chi_{\rm Kerr}$ only by a constant factor but depends only on the laser parameters like Δ_p, Δ_c, and Ω_c, as can be checked based on Eqs. (6)–(11). The calculation presented above is based on cold atoms. In the case of hot atoms, the atomic motion will introduce the Doppler effect such that the single-photon detunings Δ_p and Δ_c have to be replaced by $\Delta_p - k_pv_z$ and $\Delta_c + k_cv_z$, with $k_j = \omega_j/c$ for $j \in \{p, c\}$ being the corresponding wave number. Here, for simplicity, we have considered that the two fields propagate collinearly in the z direction. In addition, the two fields are assumed to be antiparallel with respect to each other, in order to compensate for the Doppler effect on the two-photon detuning [55]. By averaging contributions from all atoms based on the Maxwell-Boltzmann distribution, we obtain the nonlinear susceptibility for thermal atoms as

$$\chi^{(3)} = \int_{-\infty}^{\infty}\frac{f_{\rm MB}(v_z)\rho_{21}^{(3)}(v_z)}{\Omega_p^3}dv_z, \quad (14)$$

where $f_{\rm MB}(v_z) = e^{-v_z^2/v_{\rm th}^2}/\sqrt{\pi}v_{\rm th}$ is the Maxwell-Boltzmann distribution function and $\rho_{21}^{(3)}(v_z)$ is the same as $\rho_{21}^{(3)}$ except that Δ_p, Δ_c, $\rho_{11}^{(2)}$, and $\rho_{22}^{(2)}$ are now velocity dependent due to the Doppler effect. In addition, $v_{\rm th} = \sqrt{2k_BT/m}$ is the most probable velocity, where T is the temperature of the thermal atomic ensemble and m is the atomic mass.

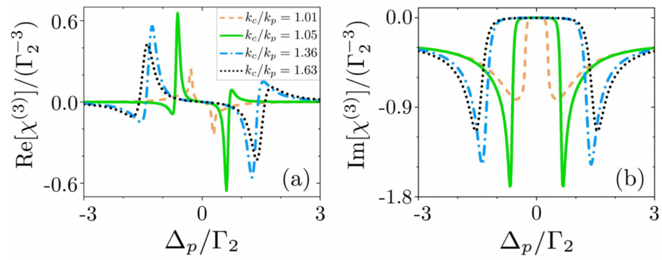

FIG. 2. Nonlinear (a) dispersion $\mathrm{Re}(\chi^{(3)})$ and (b) absorption $\mathrm{Im}(\chi^{(3)})$ as a function of Δ_p for different ratios k_c/k_p with fixed k_p. Here k_p is chosen for the D_2 transition of ^{87}Rb whose wavelength is 780.2 nm, while k_c given in increasing order corresponds to $|3\rangle$ chosen as $5D_{5/2}$, $7S_{1/2}$, $7D_{5/2}$, and $100S_{1/2}$ with associated wavelengths of 776.0, 741.0, 572.6, and 480.0 nm, respectively. These values are derived from the alkali Rydberg calculator package [61]. The parameters are $\Omega_c = 1.5\Gamma_2$, $\Gamma_3 = 0.1\Gamma_2$, $\Delta_c = 0$, and $T = 300$ K.

To investigate the effect of wave-number mismatch on the Kerr nonlinearity, we consider the probe transition as the D_2 line of ^{87}Rb, with a fixed probe wave number $k_p = 2\pi/\lambda_p$, where $\lambda_p = 780.24$ nm. The coupling wave number k_c is varied by selecting different Rydberg states $|3\rangle$ with distinct principal quantum numbers. At relatively high temperature such as room temperature or even higher, additional decoherence mechanisms such as atomic collisions, transit-time broadening, and other dephasing processes become significant [57–59]. These effects are particularly pronounced for high-lying Rydberg states, whose intrinsic spontaneous decay rates are extremely low [60]. Consequently, the total decoherence rate Γ_3 may vary for different k_c. In the following, we first assume a constant $\Gamma_3 = 0.1\Gamma_2$ to isolate the effect of wave-number mismatch; this choice corresponds to the $5D_{5/2}$ state with $k_c/k_p = 1.01$. The influence of Γ_3 on the Kerr nonlinearity will be addressed later in Fig. 6 by phenomenologically incorporating decoherence effects, which effectively increase Γ_3. We then numerically calculate Eq. (14) at room temperature $T = 300$ K. The resulting nonlinear dispersion and absorption as a function of probe detuning Δ_p are plotted in Figs. 2(a) and 2(b) for different k_c/k_p. Here k_c/k_p in increasing order corresponds to the state $|3\rangle$ chosen to be $5D_{5/2}$, $7S_{1/2}$, $7D_{5/2}$, and $100S_{1/2}$, respectively. For growing k_c/k_p, both the peak nonlinear dispersion and absorption are first enhanced and then attenuated. To illustrate such a behavior, we allow k_c to be continuously increasing, and the peak dispersion and absorption are shown in Figs. 3(a) and 3(b), respectively. In general, it can be seen that both the peak dispersion $\mathrm{Re}(\chi^{(3)})_{\rm max}$ and the absolute value of the maximal absorption $|\mathrm{Im}(\chi^{(3)})_{\rm min}|$ are simultaneously improved for the chosen range of $1 < k_c/k_p < 2.0$ as compared to the case of $k_c/k_p = 1$. For k_c/k_p slightly greater than 1, $\mathrm{Re}(\chi^{(3)})_{\rm max}$ is maximally enhanced by a factor of approximately 3, while an enhancement factor of approximately 2 can be achieved for $|\mathrm{Im}(\chi^{(3)})_{\rm min}|$. For even larger k_c/k_p, the dispersion and absorption will be reduced eventually. Nevertheless, the Kerr nonlinearity is enhanced for a certain range of k_c/k_p, which is the key result of our work.

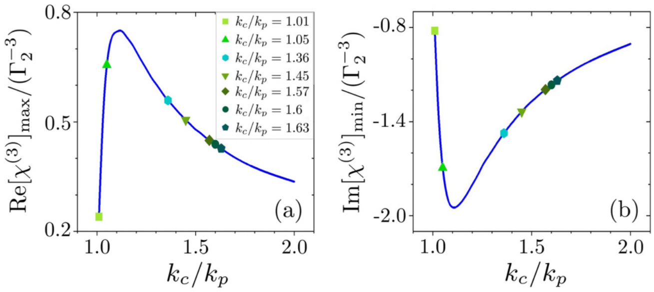

FIG. 3. Maximal third-order (a) dispersion and (b) absorption for increasing k_c/k_p with fixed k_p. The discrete data points at different k_c/k_p in increasing order correspond to $|3\rangle$ chosen as $5D_{5/2}$, $7S_{1/2}$, $7D_{5/2}$, $10S_{1/2}$, $15S_{1/2}$, $20S_{1/2}$, and $100S_{1/2}$, respectively. The wavelengths corresponding to $10S_{1/2}$, $15S_{1/2}$, and $20S_{1/2}$ are 539.2, 497.6, and 488.1 nm, respectively [61]. The other parameters are the same as in Fig. 2.

The first rising and gradually falling behavior of the enhanced Kerr nonlinearity due to the wave-number mismatch can be well explained in the dressed-state picture. The two peaks in the nonlinear absorption are associated with two probe transitions from the ground state to the two dressed states created by Ω_c [55], which for atoms moving with speed v_z are determined by the eigenstates of

$$\begin{bmatrix} -\Delta_p + k_p v_z & -\Omega_c \\ -\Omega_c & -\Delta_p - \Delta_c + (k_p - k_c)v_z \end{bmatrix}. \tag{15}$$

The eigenfrequencies are given by

$$\lambda_\pm(v_z) = k_p v_z + \frac{-k_c v_z \pm \sqrt{(k_c v_z)^2 + 4\Omega_c^2}}{2} \tag{16}$$

and the corresponding eigenvectors are

$$|\pm(v_z)\rangle = c_{2\pm}(v_z)|2\rangle + c_{3\pm}(v_z)|3\rangle, \tag{17}$$

with $c_{2\pm}$ and $c_{3\pm}$ the normalized coefficients such that $|c_{2\alpha}|^2 + |c_{3\alpha}|^2 = 1$ and $c_{2\alpha}/c_{3\alpha} = \Omega_c/(\lambda_\alpha - k_p v_z)$ for $\alpha \in \{+, -\}$. Here we have chosen $\Delta_p = \Delta_c = 0$ for simplicity.

We first plot the eigenvalues $\lambda_\pm$ as a function of v_z in Fig. 4 for different k_c/k_p, which correspond to Figs. 2(a) and 2(b). For $\Omega_c = 0$, the two eigenvalues reduce to $\lambda_+ = k_p v_z$

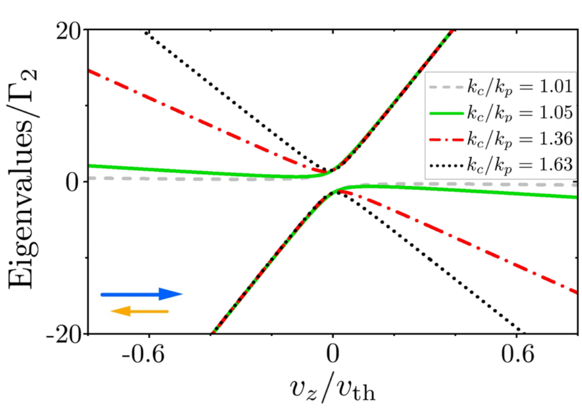

FIG. 4. Eigenvalues λ_+ (upper branch) and λ_- (lower branch) as a function of v_z for different k_c/k_p. An anticrossing appears when $k_c/k_p > 1$. Here $\Delta_p = 0$, $\Delta_c = 0$, and $\Omega_c = 1.5\Gamma_2$.

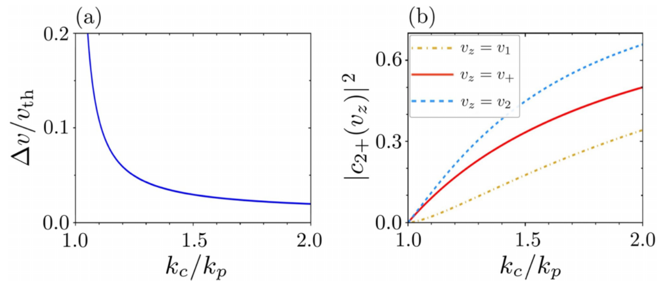

FIG. 5. (a) Velocity range Δv and (b) $|c_{2+}(v_z)|^2$ as a function of k_c/k_p for $k_c/k_p > 1$. The parameters are the same as in Fig. 2. Additionally, $v_1 = v_+ - \Gamma_2/2(k_c - k_p)$ and $v_2 = v_+ + \Gamma_2/2k_p$ in (b).

and $\lambda_- = (k_p - k_c)v_z$. Obviously, for $k_c/k_p > 1$, λ_- has a negative slope with respect to v_z. When turning on Ω_c, an anticrossing appears near $v_z = 0$, i.e., λ_+ has a local minimum while λ_- has a local maximum. The anticrossing defines a frequency gap in which the probe transition to the two dressed states is not allowed. As discussed previously, this gap corresponds to the EIT window [55], and also the spectral distance between the two dips in the nonlinear absorption spectrum. Furthermore, the spectral position of the right dip locates approximately around $\min(\lambda_+)$, which corresponds to a velocity group $v_z = v_+$, where v_+ can be determined from $d\lambda_+/dv_z = 0$, which is given by

$$v_+ = \frac{(k_c - 2k_p)\Omega_c}{k_c\sqrt{(k_c - k_p)k_p}}, \tag{18}$$

which is valid for $k_c/k_p > 1$. In a similar manner, the left dip is located approximately at $\max(\lambda_-)$, and the corresponding velocity group $v_z = v_-$ is defined by $d\lambda_-/dv_z = 0$, leading to $v_- = -v_+$.

The nonlinear absorption spectrum results from summing over the probe transitions to the two dressed states for all v_z. In particular, the right and left dips in $\mathrm{Im}(\chi^{(3)})$ are determined by the velocity groups centered at v_+ and v_-, respectively. Since the spectral width of the dips is on the order of Γ_2 as shown in Fig. 2(b), it then follows that the right dip is mainly determined by the contributions from moving atoms with detuning approximately in the range $[\min(\lambda_+) - \frac{\Gamma_2}{2}, \min(\lambda_+) + \frac{\Gamma_2}{2}]$, which is translated to a velocity range of $[v_+ - \Gamma_2/2(k_c - k_p), v_+ + \Gamma_2/2k_p]$. Similarly, the left absorption dip is determined by atomic contributions in the velocity range $[v_- - \Gamma_2/2k_p, v_- + \Gamma_2/2(k_c - k_p)]$. We notice that the sizes of the two velocity ranges are the same as each other and are given by

$$\Delta v = \frac{\Gamma_2}{2k_p}\left(1 + \frac{k_p}{k_c - k_p}\right). \tag{19}$$

As shown in Fig. 5(a), it can be seen that Δv decreases rapidly for increasing k_c/k_p.

The nonlinear peak absorption is not only determined by the number of atoms involved in the interaction which is governed by Δv, but also dependent on the effective transition strength between the ground and dressed states, which is proportional to the absolute square of the coefficient of the component $|2\rangle$ in $|\pm\rangle$, i.e., $|c_{2\pm}(v_z)|^2$. As a result, the height of the absorption plotted in Fig. 3(b) is dominated by $|c_{2\pm}(v_z)|^2$

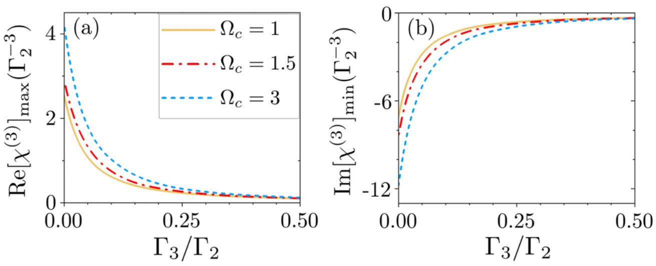

FIG. 6. Maximal nonlinear (a) dispersion and (b) absorption as a function of Γ_3 for different Ω_c. The parameters are the same as in Fig. 2 except that $k_c/k_p = 1.12$, which is the ratio corresponding to maximal enhancement of Kerr nonlinearity.

for v_z in the velocity range presented above. In this narrow range Δv, $|c_{2+}(v_z)|^2$ becomes larger for increasing k_c/k_p, as shown in Fig. 5(b) , where we have plotted $|c_{2+}(v_z)|^2$ for three different velocities $v_1 = v_+ - \Gamma_2/2(k_c - k_p)$, v_+, and $v_2 = v_+ + \Gamma_2/2k_p$. It can be checked that similar behavior can be also found for $|c_{2-}(v_z)|^2$. The increasing $|c_{2\pm}(v_z)|^2$ would enhance $|\mathrm{Im}(\chi^{(3)})_{\min}|$. However, with increasing k_c/k_p, the velocity range Δv that contributes to $|\mathrm{Im}(\chi^{(3)})_{\min}|$ becomes narrower, as shown in Fig. 5(a) , indicating that fewer atoms participate in the interaction, which tends to reduce the peak nonlinear absorption. The competition between the amplified coefficients $|c_{2\pm}(v_z)|^2$ and the narrowing velocity range Δv for increasing k_c/k_p leads to an initial increase followed by a gradual reduction in $|\mathrm{Im}(\chi^{(3)})_{\min}|$, as shown in Fig. 3(b) . Accordingly, $\mathrm{Re}(\chi^{(3)})_{\max}$ follows a similar behavior, as shown in Fig. 3(a) . We notice that the width of the EIT window varies in a similar manner as a function of k_c/k_p, as has been shown in previous work [55]. However, we have identified the physical mechanism underlying this behavior as resulting from the competition between transition strength and effective atom number.

In the preceding discussion, we assumed a small and constant Γ_3 for different k_c to facilitate a direct comparison. However, in room-temperature alkali-metal atoms, atomic motion introduces additional decoherence effects that become important for higher-lying Rydberg states $|3\rangle$, even though their spontaneous decay rates are low [60]. To account for this, we now incorporate these effects phenomenologically and present $\mathrm{Re}(\chi^{(3)})_{\max}$ and $\mathrm{Im}(\chi^{(3)})_{\min}$ as a functios of Γ_3 in Fig. 6. In general, a larger Γ_3 corresponds to stronger dissipation, which in turn reduces the Kerr nonlinearity.

III. DISCUSSION AND CONCLUSION

In analyzing the effect of wave-number mismatch on the Kerr nonlinearity, we have assumed a constant control Rabi frequency. For larger k_c, which corresponds to a smaller dipole moment for the upper transition, this implies the need for a stronger control field to maintain the same Rabi frequency. Fortunately, the maximal enhancement of the Kerr nonlinearity occurs near $k_c/k_p \simeq 1.1$, where the dipole moment for the upper transition is not substantially smaller than that at $k_c/k_p \simeq 1$. This suggests that the enhancement effect due to wave-number mismatch is experimentally verifiable in practical conditions.

We have theoretically analyzed the Kerr nonlinearity including both nonlinear dispersion and absorption in hot atomic ensemble under ladder-type EIT configuration. The control and probe fields are assumed in an antiparallel geometry to compensate for the two-photon Doppler effect and subsequently enable an EIT-like nonlinear spectrum for the probe field. When the wave number of the control field exceeds that of the probe field, i.e., $k_c > k_p$, the eigenvalues of the two dressed states for a nonzero control field exhibit an avoided crossing with respect to velocities, respectively, effectively creating a frequency gap which corresponds to the transparency window for the probe field. For increasing k_c/k_p, the transition strength to the two dressed states around the avoided crossing is amplified, whereas there are fewer atoms contributing to the nonlinearity. As a result of the interplay between these two mechanisms, the Kerr nonlinearity including both the maximal dispersion and absorption features an initial increase followed by a gradual reduction. Nevertheless, both the dispersion and absorption are enhanced as compared to the case of $k_c = k_p$ in the considered regime $1 < k_c/k_p < 2$. An optimal enhancement can be easily achieved when k_c slightly exceeds k_p, due to the two competing mechanisms explained above. In principle, our results may facilitate nonlinear optical applications in both classical and quantum regimes using hot atomic vapors. While incorporating our findings with quantum applications would require a more comprehensive analysis of additional decoherence effects, which lies beyond the scope of the present work, our results are directly applicable to classical nonlinear optical phenomena. These include the realizations of self-phase modulation [2–5], optical solitons [6–10], and optical bistability [11–14] at reduced probe power.

ACKNOWLEDGMENTS

This work was supported by the Quantum Science and Technology–National Science and Technology Major Project (Grant No. 2021ZD0300802), the National Natural Science Foundation of China (Grants No. 12034007 and No. 12374327), Major Project of Shanghai Municipal Education Commission (Grant No. 2023ZKZD39), and Program of Shanghai Academic Research Leader (Grant No. 21XD1400700).

DATA AVAILABILITY

The data that support the findings of this article are not publicly available upon publication because it is not technically feasible and/or the cost of preparing, depositing, and hosting the data would be prohibitive within the terms of this research project. The data are available from the authors upon reasonable request.

[1] R. W. Boyd, *Nonlinear Optics* (Academic, New York, 2020).

[2] R. H. Stolen and C. Lin, Self-phase-modulation in silica optical fibers, Phys. Rev. A **17**, 1448 (1978).

[3] F. Parmigiani, C. Finot, K. Mukasa, M. Ibsen, M. A. F. Roelens, P. Petropoulos, and D. J. Richardson, Ultra-flat SPM-broadened spectra in a highly nonlinear fiber using parabolic pulses formed in a fiber Bragg grating, Opt. Express **14**, 7617 (2006).
[4] N. Vermeulen, D. Castelló-Lurbe, J. Cheng, I. Pasternak, A. Krajewska, T. Ciuk, W. Strupinski, H. Thienpont, and J. Van Erps, Negative Kerr nonlinearity of graphene as seen via chirped-pulse-pumped self-phase modulation, Phys. Rev. Appl. **6**, 044006 (2016).
[5] A. Zheltikov, Analytical insights into self-phase modulation: Beyond the basic theory, Opt. Express **26**, 17571 (2018).
[6] J. S. Aitchison, A. M. Weiner, Y. Silberberg, M. K. Oliver, J. L. Jackel, D. E. Leaird, E. M. Vogel, and P. W. E. Smith, Observation of spatial optical solitons in a nonlinear glass waveguide, Opt. Lett. **15**, 471 (1990).
[7] G. A. Swartzlander and C. T. Law, Optical vortex solitons observed in Kerr nonlinear media, Phys. Rev. Lett. **69**, 2503 (1992).
[8] A. Ciattoni, B. Crosignani, P. D. Porto, and A. Yariv, Perfect optical solitons: Spatial Kerr solitons as exact solutions of Maxwell's equations, J. Opt. Soc. Am. B **22**, 1384 (2005).
[9] Q. Zhou, M. Mirzazadeh, M. Ekici, and A. Sonmezoglu, Analytical study of solitons in non-Kerr nonlinear negative-index materials, Nonlinear Dyn. **86**, 623 (2016).
[10] K. Hosseini, M. Mirzazadeh, D. Baleanu, S. Salahshour, and L. Akinyemi, Optical solitons of a high-order nonlinear Schrödinger equation involving nonlinear dispersions and Kerr effect, Opt. Quantum Electron. **54**, 177 (2022).
[11] I. E. Protsenko and A. V. Uskov, Single-photon optical bistability in a small nonlinear cavity, Phys. Rev. A **108**, 023724 (2023).
[12] Z. Wang, X.-K. Jiang, H.-M. Li, B.-H. Yang, C. Jiang, and H.-C. Yuan, Optical bistability at lower photon number via photon and phonon interaction in the presence of Kerr nonlinearity, Laser Phys. **34**, 075201 (2024).
[13] L. T. Y. Nga, N. H. Bang, N. V. Phu, H. M. Dong, N. T. T. Hien, N. V. Ai, and L. V. Doai, Variable Kerr nonlinearity and optical bistability of a four-level lambda atomic medium, Chaos Soliton. Fract. **191**, 115870 (2025).
[14] P. Tritschler, C. Schweikert, R. H. Klenk, S. Abdani, O. Sözen, W. Vogel, G. Rademacher, T. Ohms, A. Zimmermann, and P. Degenfeld-Schonburg, Nonlinear optical bistability in microring resonators for enhanced phase sensing, Phys. Rev. Lett. **134**, 123802 (2025).
[15] Š. Bräuer and P. Marek, Generation of quantum states with nonlinear squeezing by Kerr nonlinearity, Opt. Express **29**, 22648 (2021).
[16] N. Kalinin, T. Dirmeier, A. A. Sorokin, E. A. Anashkina, L. L. Sánchez-Soto, J. F. Corney, G. Leuchs, and A. V. Andrianov, Observation of robust polarization squeezing via the Kerr nonlinearity in an optical fiber, Adv. Quantum Technol. **6**, 2200143 (2023).
[17] N. Kalinin, T. Dirmeier, A. A. Sorokin, E. A. Anashkina, L. L. Sánchez-Soto, J. F. Corney, G. Leuchs, and A. V. Andrianov, Quantum-enhanced interferometer using Kerr squeezing, Nanophotonics **12**, 2945 (2023).
[18] S. Y. Song, S. Wang, G. F. Xu, and G. L. Long, Entanglement generation with coherent states using cross-Kerr nonlinearity, J. Opt. Soc. Am. B **30**, 2393 (2013).
[19] Z. Zhang, M. O. Scully, and G. S. Agarwal, Quantum entanglement between two magnon modes via Kerr nonlinearity driven far from equilibrium, Phys. Rev. Res. **1**, 023021 (2019).
[20] C. Silberhorn, P. K. Lam, O. Weiß, F. König, N. Korolkova, and G. Leuchs, Generation of continuous variable Einstein-Podolsky-Rosen entanglement via the Kerr nonlinearity in an optical fiber, Phys. Rev. Lett. **86**, 4267 (2001).
[21] N. Imoto, H. A. Haus, and Y. Yamamoto, Quantum nondemolition measurement of the photon number via the optical Kerr effect, Phys. Rev. A **32**, 2287 (1985).
[22] I. Fushman and J. Vučković, Analysis of a quantum nondemolition measurement scheme based on Kerr nonlinearity in photonic crystal waveguides, Opt. Express **15**, 5559 (2007).
[23] Y.-F. Xiao, Ş. K. Özdemir, V. Gaddam, C.-H. Dong, N. Imoto, and L. Yang, Quantum nondemolition measurement of photon number via optical Kerr effect in an ultra-high-Q microtoroid cavity, Opt. Express **16**, 21462 (2008).
[24] S. E. Harris, J. E. Field, and A. Imamoğlu, Nonlinear optical processes using electromagnetically induced transparency, Phys. Rev. Lett. **64**, 1107 (1990).
[25] K.-J. Boller, A. Imamoğlu, and S. E. Harris, Observation of electromagnetically induced transparency, Phys. Rev. Lett. **66**, 2593 (1991).
[26] M. Fleischhauer and M. D. Lukin, Dark-state polaritons in electromagnetically induced transparency, Phys. Rev. Lett. **84**, 5094 (2000).
[27] M. Fleischhauer and M. D. Lukin, Quantum memory for photons: Dark-state polaritons, Phys. Rev. A **65**, 022314 (2002).
[28] C. Liu, Z. Dutton, C. H. Behroozi, and L. V. Hau, Observation of coherent optical information storage in an atomic medium using halted light pulses, Nature (London) **409**, 490 (2001).
[29] D. F. Phillips, A. Fleischhauer, A. Mair, R. L. Walsworth, and M. D. Lukin, Storage of light in atomic vapor, Phys. Rev. Lett. **86**, 783 (2001).
[30] M. Fleischhauer, A. Imamoglu, and J. P. Marangos, Electromagnetically induced transparency: Optics in coherent media, Rev. Mod. Phys. **77**, 633 (2005).
[31] A. V. Gorshkov, A. André, M. D. Lukin, and A. S. Sørensen, Photon storage in Λ-type optically dense atomic media. II. Free-space model, Phys. Rev. A **76**, 033805 (2007).
[32] H. Schmidt and A. Imamoglu, Giant Kerr nonlinearities obtained by electromagnetically induced transparency, Opt. Lett. **21**, 1936 (1996).
[33] L. Deng, M. G. Payne, and W. R. Garrett, Electromagnetically-induced-transparency-enhanced Kerr nonlinearity: Beyond steady-state treatment, Phys. Rev. A **64**, 023807 (2001).
[34] H. Kang and Y. Zhu, Observation of large Kerr nonlinearity at low light intensities, Phys. Rev. Lett. **91**, 093601 (2003).
[35] Y. Niu, S. Gong, R. Li, Z. Xu, and X. Liang, Giant Kerr nonlinearity induced by interacting dark resonances, Opt. Lett. **30**, 3371 (2005).
[36] Y. Niu and S. Gong, Enhancing Kerr nonlinearity via spontaneously generated coherence, Phys. Rev. A **73**, 053811 (2006).
[37] H. Sun, Y. Niu, S. Jin, and S. Gong, Phase control of the Kerr nonlinearity in electromagnetically induced transparency media, J. Phys. B **41**, 065504 (2008).
[38] D. X. Khoa, L. V. Doai, D. H. Son, and N. H. Bang, Enhancement of self-Kerr nonlinearity via electromagnetically induced transparency in a five-level cascade system: An analytical approach, J. Opt. Soc. Am. B **31**, 1330 (2014).

[39] D. D. Yavuz and D. E. Sikes, Giant Kerr nonlinearities using refractive-index enhancement, Phys. Rev. A **81**, 035804 (2010).

[40] X. Yang, S. Li, C. Zhang, and H. Wang, Enhanced cross-Kerr nonlinearity via electromagnetically induced transparency in a four-level tripod atomic system, J. Opt. Soc. Am. B **26**, 1423 (2009).

[41] H. R. Hamedi, A. H. Gharamaleki, and M. Sahrai, Colossal Kerr nonlinearity based on electromagnetically induced transparency in a five-level double-ladder atomic system, Appl. Opt. **55**, 5892 (2016).

[42] J. Sinclair, D. Angulo, N. Lupu-Gladstein, K. Bonsma-Fisher, and A. M. Steinberg, Observation of a large, resonant, cross-Kerr nonlinearity in a cold Rydberg gas, Phys. Rev. Res. **1**, 033193 (2019).

[43] Y. Mu, L. Qin, Z. Shi, and G. Huang, Giant Kerr nonlinearities and magneto-optical rotations in a Rydberg-atom gas via double electromagnetically induced transparency, Phys. Rev. A **103**, 043709 (2021).

[44] M. Xiao, Y.-q. Li, S.-z. Jin, and J. Gea-Banacloche, Measurement of dispersive properties of electromagnetically induced transparency in rubidium atoms, Phys. Rev. Lett. **74**, 666 (1995).

[45] G. Vemuri and G. S. Agarwal, Role of inhomogeneous broadening in lasing without inversion in ladder systems, Phys. Rev. A **53**, 1060 (1996).

[46] S. D. Badger, I. G. Hughes, and C. S. Adams, Hyperfine effects in electromagnetically induced transparency, J. Phys. B **34**, L749 (2001).

[47] A. K. Mohapatra, T. R. Jackson, and C. S. Adams, Coherent optical detection of highly excited Rydberg states using electromagnetically induced transparency, Phys. Rev. Lett. **98**, 113003 (2007).

[48] H. R. Noh and H. S. Moon, Analytical solutions of the susceptibility for Doppler-broadened three-level atomic systems, J. Phys. B **45**, 245002 (2012).

[49] A. Urvoy, C. Carr, R. Ritter, C. S. Adams, K. J. Weatherill, and R. Löw, Optical coherences and wavelength mismatch in ladder systems, J. Phys. B **46**, 245001 (2013).

[50] J. Gea-Banacloche, Y.-q. Li, S.-z. Jin, and M. Xiao, Electromagnetically induced transparency in ladder-type inhomogeneously broadened media: Theory and experiment, Phys. Rev. A **51**, 576 (1995).

[51] S. Shepherd, D. J. Fulton, and M. H. Dunn, Wavelength dependence of coherently induced transparency in a Doppler-broadened cascade medium, Phys. Rev. A **54**, 5394 (1996).

[52] J. R. Boon, E. Zekou, D. McGloin, and M. H. Dunn, Comparison of wavelength dependence in cascade-, Λ-, and Vee-type schemes for electromagnetically induced transparency, Phys. Rev. A **59**, 4675 (1999).

[53] A. B. Mirza and S. Singh, Wave-vector mismatch effects in electromagnetically induced transparency in Y-type systems, Phys. Rev. A **85**, 053837 (2012).

[54] N. Thaicharoen, K. R. Moore, D. A. Anderson, R. C. Powel, E. Peterson, and G. Raithel, Electromagnetically induced transparency, absorption, and microwave-field sensing in a Rb vapor cell with a three-color all-infrared laser system, Phys. Rev. A **100**, 063427 (2019).

[55] L. Zhang, N. Stiesdal, H. Busche, M. G. Hansen, T. Pohl, and S. Hofferberth, Interplay of electromagnetically induced transparency and Doppler broadening in hot atomic vapors, New J. Phys. **26**, 075002 (2024).

[56] M. O. Scully and M. S. Zubairy, *Quantum Optics* (Cambridge University Press, Cambridge, 1997).

[57] I. Novikova, R. L. Walsworth, and Y. Xiao, Electromagnetically induced transparency-based slow and stored light in warm atoms, Laser Photonics Rev. **6**, 333 (2012).

[58] A. J. van Lange, P. van der Straten, and D. van Oosten, Combined effect of non-linear optical and collisional processes on absorption saturation in a dense rubidium vapour, J. Phys. B **53**, 125402 (2020).

[59] R. Finkelstein, S. Bali, O. Firstenberg, and I. Novikova, A practical guide to electromagnetically induced transparency in atomic vapor, New J. Phys. **25**, 035001 (2023).

[60] W. Li, I. Mourachko, M. W. Noel, and T. F. Gallagher, Millimeter-wave spectroscopy of cold Rb Rydberg atoms in a magneto-optical trap: Quantum defects of the *ns*, *np*, and *nd* series, Phys. Rev. A **67**, 052502 (2003).

[61] N. Šibalić, J. Pritchard, C. Adams, and K. Weatherill, ARC: An open-source library for calculating properties of alkali Rydberg atoms, Comput. Phys. Commun. **220**, 319 (2017).